ELSEVIER

1 January 2000

Optics Communications 173 (2000) 145–153

OPTICS COMMUNICATIONS

www.elsevier.com/locate/optcom

Patterns in Mie scattering

C.M. Sorensen *, D.J. Fischbach

Program for Complex Fluid Flows and Department of Physics, Kansas State University, Manhattan, KS 66506-2601, USA

Received 4 August 1999; accepted 14 October 1999

Abstract

This work demonstrates that heretofore undisclosed patterns emerge when the Mie scattered intensity for an arbitrary sphere of radius R and refractive index m is plotted versus the dimensionless parameter qR, where $q = 4\pi\lambda^{-1}\sin(\theta/2)$ is the scattering wavevector at scattering angle θ for wavelength λ. When the interference ripple structure is ignored, three power law regimes can appear. These regimes are dependent on the phase shift parameter $\rho = 2kR|m-1|$, where k is the wave number, with the behavior having universal aspects for a given ρ. To explain these patterns use is made of a general concept that the scattered intensity is the square of the Fourier transform, i.e., the structure factor, of the illuminated portion of the scattering object. If we make an approximation that the illuminate portion of the sphere is an annular shell at large ρ, Fourier transformation of the shell and scaling arguments can explain these power laws and the length scales associated with their crossovers. However, such an approximation is severe and an exact explanation of the new patterns is still lacking.

PACS: 3.80.+r; 42.25.Fx; 78.35+c
Keywords: Light scattering; Mie scattering

1. Introduction

The problem of how light, or electromagnetic radiation in general, scatterers from a sphere of arbitrary size and refractive index was solved more than 90 years ago through the efforts of a number of workers, most notably Mie, Lorentz and Debye. The result, often called Lorentz–Mie theory or simply Mie scattering, gives the scattered intensity as a function of scattering angle for arbitrary polarization [1–3]. The equations that describe this scattering are quite complex, not withstanding the simplicity of the spherically symmetric homogeneous sphere, involving sums over associated Legendre polynomials with coefficients that involve Ricatti–Bessel and Hankel functions. Because of this complexity, numerical results were once very difficult to obtain, and only with the advent of modern computational machines are Mie scattering values easily computed. This complexity, however, still obscures the physical meaning and interpretation of the scattering.

In this paper we show that by plotting the scattered light intensity versus the scattering wavevector, rather than the scattering angle, patterns emerge which, to our knowledge, have not been described before in the literature. These patterns involve the envelopes of the scattering curves and evolve in a

* Corresponding author. Tel.: +1-785-532-1626; fax: +1-785-532-6806; e-mail: sor@phys.ksu.edu

0030-4018/00/$ - see front matter
PII: S0030-4018(99)00624-0

coherent fashion from the Rayleigh–Debye–Gans limit of the Mie results. The evolution is controlled by the phase shift parameter (Eq. (3b), below). Having established this empirical result, we successfully replicate the patterns with a model that localizes the electromagnetic field to an annular shell within the sphere, the thickness of which decreases with increasing phase shift parameter. However, previous workers have shown that while there is some tendency for the internal field to localize near the inner surface, our model is too simple, hence a complete explanation of the patterns remains to be achieved.

2. Mie scattering curves

We limit ourselves to the problem of scattering by a homogeneous, dielectric sphere of arbitrary radius R and real refractive index m relative to the medium. The scattering geometry is also limited to detect the scattered intensity I due to vertically polarized incident and scattered light with a horizontal scattering plane. This plane is defined by the plane of the incident ($\vec{k}_i$) and scattered ($\vec{k}_s$) wave vectors, i.e., the scattering angle θ is in the horizontal plane. The scattering is elastic so both wave vectors have a magnitude $k = 2\pi/\lambda$ where λ is the wavelength. This is the typical laser light scattering set-up. To create I vs. θ 'data' we use a standard Mie scattering algorithm, BHMIE, given by Bohren and Huffman [3].

Fig. 1(a) shows an example of Mie scattering for an index of refraction $m = 1.05$ and a variety of sizes expressed as the size parameter kR. The normalized intensity $I(\theta)/I(0)$ vs. θ is plotted. A profusion of bumps and wiggles are seen with some periodicities, but with no particularly coherent pattern. Curves for the larger $m = 1.50$ in Fig. 2(a) are even more complex. A major point of this paper, however, is that θ, although conveniently measured in the laboratory, is not the most propitious parameter for plotting the data. It is well known from other scattering phenomena, such as X-ray and neutron scattering [4–6], that the scattering wave vector, $\vec{q} = \vec{k}_s - \vec{k}_i$, with magnitude

$$q = 4\pi\lambda^{-1} \sin\theta/2 \qquad (1)$$

is a useful independent variable for describing scattering. One may cite at least two reasons for the usefulness of q: (1) it results naturally from the theory for scattering of waves of any type. Scattering theory finds that the scattered amplitude is the Fourier transform of the real space structure and q is the Fourier transform variable; and (2) its units are inverse length, hence its inverse, q^{-1}, is the length scale, or probe length, of the scattering [7]. Given this latter aspect, q can be combined with R, the length scale of the scatterer, to yield a dimensionless variable qR. If universal features reside in Mie scattering, they may reveal themselves in a plot of normalized intensity vs. qR. We note that such an analysis is not new, but, remarkably, its application to Mie scattering appears to be.

Fig. 1(b) and Fig. 2(b) plot the data of Fig. 1(a) and Fig. 2(a) vs. qR. Definite patterns emerge, some of which are well know. At small qR a nearly universal 'forward scattering lobe' is seen. Near $qR \sim 1$, the fall off is approximately described by the Guinier equation $I(q)/I(0) \sim 1 - q^2R^2/5$. After that, we see patterns less familiar. For $m = 1.05$ the periodicity of the interference ripples is $\Delta(qR) = \pi$ which can be understood with simple interference arguments. For larger m the periodicity is more complex. The enhanced backscattering, the 'glory', visible in plots with $m = 1.50$, shows no particular pattern but is compressed into the large qR part fo each size parameter kR. The key features to be explored here are the envelopes of these plots. Fig. 1(b) and Fig. 2(b) include lines which roughly describe these envelopes. For small size parameter kR the envelope is described by a negative four slope, hence $(qR)^{-4}$; for larger kR two slopes are seen to imply $(qR)^{-2}$ crossing over to $(qR)^{-4}$, and for $m = 1.50$ the envelope is dominated by a negative two slope although a negative four slope is visible at large qR.

Before proceeding with a study of the envelopes of the Mie scattering curves, it is valuable to recall the Rayleigh–Debye–Gans (RDG) theory for scattering from a sphere [1–3], because the Mie theory reduces to RDG in the limit of a small refractive index and phase shift parameter, Eqs. (3a) and (3b), below. The normalized scattered RDG intensity is

$$I(q)/I(0) = \left[3(\sin u - u\cos u)/(u)^3\right]^2 \qquad (2a)$$

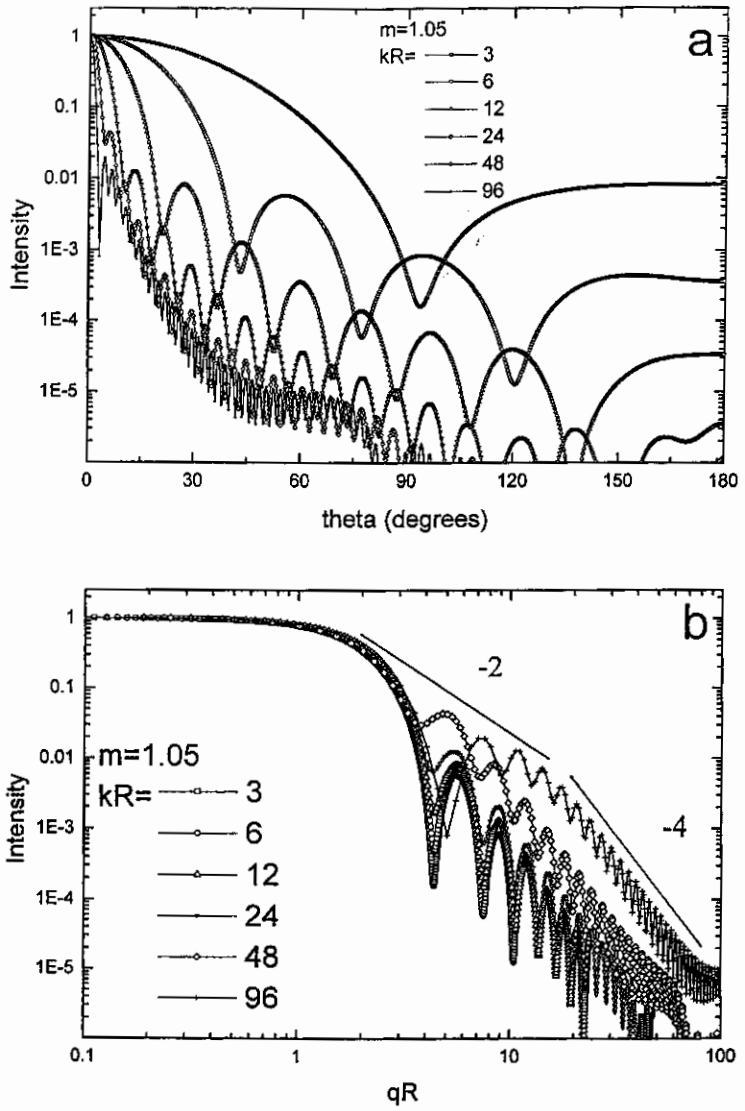

Fig. 1. (a) Normalized Mie scattering curves as a function of scattering angle for spheres of refractive index $m = 1.05$ and a variety of size parameters; and (b) same as (a) but plotted versus qR. Lines with slope -2 and -4 are shown.

where

$$u = qR. \tag{2b}$$

The RDG form is simply the square of the Fourier transform of the uniform sphere, and in this sense it is the structure factor of the uniform sphere, since this is equivalent to the Fourier transform of the density autocorrelation function. It has an envelope proportional to $(qR)^{-4}$ for large qR. It is valid in the limit where the phase shift of the wave across the sphere is not much different than the phase shift in the absence of the sphere. The difference in phase shifts is $2kR|m-1|$, the phase shift parameter ρ [1], and the condition for RDG of Eqs. (2a) and (2b) to hold is both

$$|m-1| < 1 \tag{3a}$$

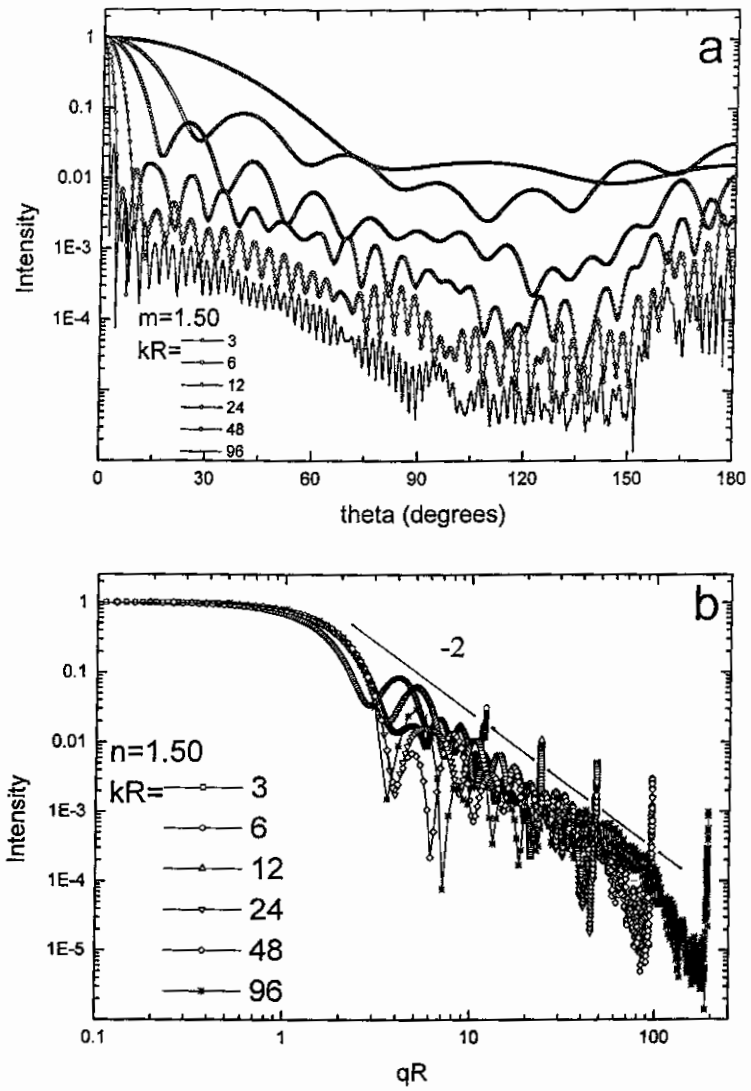

Fig. 2. (a) Normalized Mie scattering curves as a function of scattering angle for spheres of refractive index $m = 1.50$ and a variety of size parameters; and (b) same as (a) but plotted versus qR. Line with slope -2 is shown.

and

$$\rho = 2kR|m-1| < 1. \tag{3b}$$

To study the behavior of the Mie scattering envelopes the interference ripples and the glory near $\theta = 180°$ are ignored, only the maxima of the ripples are plotted to yield the envelopes. Fig. 3 shows the envelopes of scattering curves for three size parameters kR, but all with the same phase shift parameter $2kR|m-1|$. The data show the two power law regimes seen in Fig. 1(b) and Fig. 2(b), an initial $(qR)^{-2}$ then a crossover at large qR to $(qR)^{-4}$. In addition, universal behavior is seen in the $(qR)^{-2}$ regime with the data for different size parameters overlapping. Careful analysis of this and other plots (e.g., Fig. 2(b)) shows that there is no overlap for different size parameters in the $(qR)^{-4}$ regime.

A complete picture comes together in Fig. 4 where the envelopes for a wide range of phase shift parameters are plotted. The picture starts at $\rho = 0$

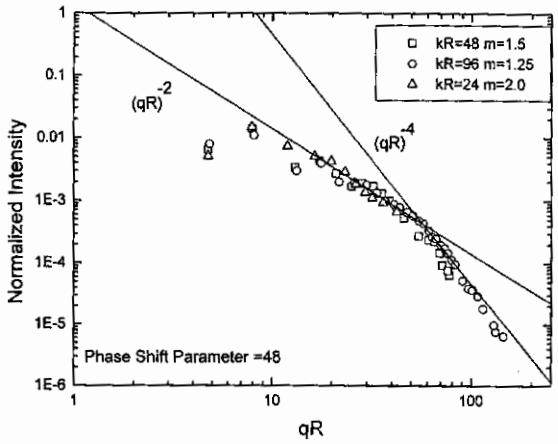

Fig. 3. The envelopes of the normalized Mie scattering curves for spheres for three different size parameters kR and refractive indices m but constrained to all have the same phase shift parameter $\rho = 2kR|m-1|$.

which is the RDG limit. As the phase shift parameter increases, the $(qR)^{-4}$ envelope moves up and away from the RDG limit at $9(qR)^{-4}$. However, it appears that this upward evolution is bounded from above by a universal $(qR)^{-2}$ power law with a coefficient approximately equal to two. Thus some envelopes, such as those for $\rho = 12$, 24, 48 (in Fig. 3), and 96 have two power law regimes as described above: $(qR)^{-2}$ and $c(qR)^{-4}$ where $c > 9$. Empirically, we find the crossover occurs approximately at $qR \simeq \rho^{-1}$, but this varies slowly with kR as evidenced by the lack of overlap in the $(qR)^{-4}$ regime for large ρ. We remark that past evaluation of Mie scattering has emphasized the importance of the size parameter kR, we now see that the phase shift parameter is also quite significant. What is the explanation of these two power laws and the reason for the crossover?

3. Interpretation

We attempt to address the question posed in the last paragraph with two equivalent approaches, a scaling argument and a Fourier transform. Both rely upon an understanding of how the optical field is

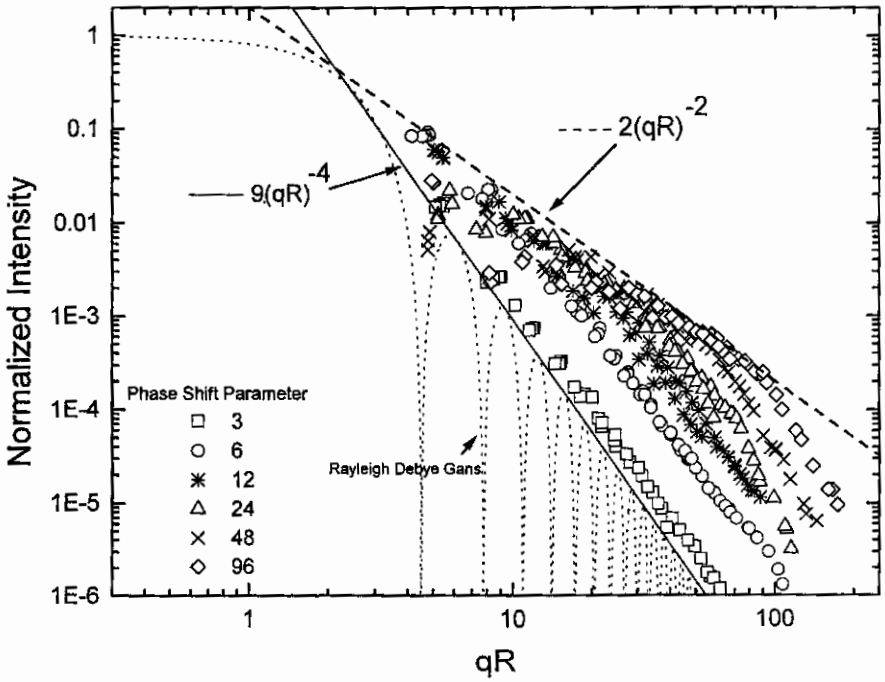

Fig. 4. The envelopes of the normalized Mie scattering curves for a wide range of size parameters and refractive indices versus qR. Curves with the same phase shift parameter fall together. As the phase shift parameter increases from zero, the curves depart from the Rayleigh–Debye–Gans limit. Lines representing $9(qR)^{-4}$ and $2(qR)^{-2}$ indicate small ρ and large ρ limits, respectively, for these curves.

distributed throughout the volume of the scattering sphere. With regard to this distribution, we will make a simplification that does not appear accurate yet does reproduce the patterns observed. The scaling argument is presented first.

Oh and Sorensen [8] have recently presented a simple, physical scaling argument to explain wave scattering from an arbitrary system of scatterers. In this approach the sphere is represented as a uniform system of point-like scatterers with spacing much less than the sphere radius as in Fig. 5 (right side). When $\rho = 0$, an incident wave scatters from each of these scatterers equally and, since they are point-like, isotropically in the scattering plane. These waves add up to create a scattered wave with amplitude

$$E(q) \propto \sum_{j}^{N} e^{i\vec{q}\cdot\vec{r}_j}. \tag{4}$$

In Eq. (4) r_j is the position of the jth scatterer within the sphere. When q is small such that $q^{-1} > R$, i.e., $qR < 1$, all the waves scatter in phase, then $E \sim N$ and $I(0) \sim N^2 \sim R^6$ and there is no q (hence θ) dependence. This explains the forward scattering lobe. As θ increases, q increases and q^{-1} decreases. When $q^{-1} < R$, the spherical system of scatterers can be broken up into touching regions of radius q^{-1}, as drawn in the right side of Fig. 5. Each of these 'q-regions' has N_q scatterers in it, and since these scatterers are all within q^{-1} of each other, they scatter in phase. Then $E \sim N_q$ so that $I_q \sim N_q^2$. N_q is proportional to the volume of the q-region so that

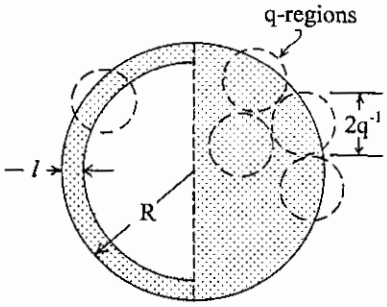

Fig. 5. Schematic of a system of point-like scatterers in a spherical particle of radius R. Also drawn are q-regions of radius q^{-1}. The right side is the uniformly illuminated, $\rho = 0$ case, where ρ is the phase shift parameter. The left size represents the large ρ situation in which the illumination is confined to a surface layer of thickness ℓ.

$N_q \sim (q^{-1})^3$ thus $I_q \sim q^{-6}$. Since the interior of the sphere (a region at a depth of q^{-1} or greater) is uniform, no total finite angle scattering results from the interior, a consequence of the Ewald–Oseen extinction theorem (only fluctuations scatter light) [9]; hence only scattering from the surface is seen. The number of q-regions on the surface is $R^2/(q^{-1})^2 = (qR)^2$. Since the q-regions are farther apart than q^{-1}, their scattered waves add randomly hence the scattered intensity is proportional to their number $(qR)^2$. Then the total scattered intensity is the product of the number of q-regions on the surface and the scattering per q-region to yield

$$I \propto R^2 q^{-4}, \quad q > R^{-1}. \tag{5}$$

This scaling argument successfully reproduces Porod's law [4,10] which predicts the scattering is proportional to q^{-4} and the surface area of the sphere. Eq. (5) when normalized by $I(0) \sim R^6$ yields

$$I(q)/I(0) \propto (qR)^{-4}, \quad q > R^{-1}, \tag{6}$$

which successful explains the power law seen in Fig. 4 for small ρ.

Any crossover between dependencies of I vs. q implies a length scale in the scattering system of magnitude q_c^{-1}, where q_c is the q-value of the crossover. For example, the crossover near $qR \sim 1$, where $I \sim q^0$ (the Rayleigh regime) crosses over to a q-dependent regime, is well known to be due to the finite size of the sphere. Figs. 3 and 4 show a new crossover at large qR which we find empirically to be $q_c^{-1} \sim R/\rho \ll R$. What is the length scale q_c^{-1}? It is known that as ρ increases for a sphere, the internal electromagnetic field inside the sphere is no longer uniform and tends to localized near the inner surface of the sphere, and the field in the interior diminishes [11–13]. For our analysis we greatly simplify the internal field as localized to a layer of width ℓ just within the surface of the sphere. This is shown schematically on the left side of Fig. 5. We have also drawn for this side of Fig. 5 a q-region of intermediate size, that is $R > q^{-1} > \ell$. In this case the number of q-regions will be as above for Porod scattering, $(qR)^2$. But now the number of illuminated scatterers in the q-region will not be proportional to the q-region volume. Instead, the roughly 2d layer of illuminated scatterers along the inner surface of the sphere

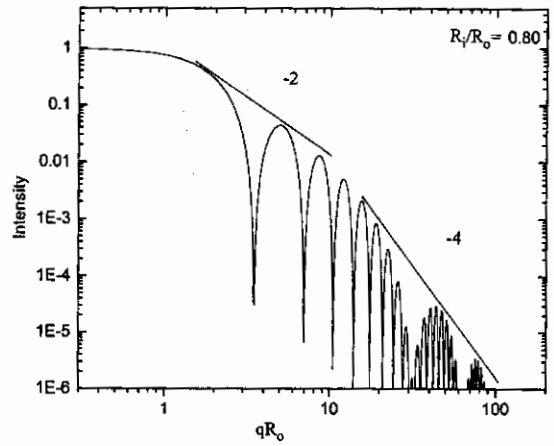

Fig. 6. Scattered intensity given by Eq. (9a) versus qR_o for a spherical shell of inner and outer radii R_i and R_o, respectively.

will be intersected by the q-regions to form circular 2d layers (like cookies with a cookie cutter). Then the number of illuminated scatterers in the q-region N_q is proportional to $(q^{-1})^2$, hence the scattered intensity per q-region will go as $I_q \sim q^{-4}$. Combining this with the number of q-regions we find

$$I \propto R^2 q^{-2}, \quad \ell^{-1} > q > R^{-1}. \tag{7}$$

Since the interior of the sphere is not illuminated at large ρ, the zero angle scattering is the in phase addition of waves from only the illuminate surface layer, hence $E \sim R^2$ and $I(0) \sim R^4$. Then normalization of Eq. (7) yields

$$I(q)/I(0) \propto (qR)^{-2}, \quad \ell^{-1} > q > R^{-1}. \tag{8a}$$

This successfully explains the dependency for large ρ at intermediate qR seen in Fig. 4. Finally, when q^{-1} becomes smaller than the layer thickness ℓ, it cannot see the layer and the Porod law, Eq. (5) returns at $q > \ell^{-1}$. However, normalization at large ρ is by $I(0) \sim R^4$ which, when applied to Eq. (5) yields

$$I(q)/I(0) \propto R^2 (qR)^{-4}, \quad q > \ell^{-1}. \tag{8b}$$

This explains both the -4 power law in this regime and the lack of data overlap for different kR values.

It is interesting that van de Hulst [1] presented a rigorous argument that in the limit of $kR \to \infty$, $m \to 1$, and $\theta \to 0$, the scattering function approaches a limit that is a function of ρ and z only, where $z = kR\theta$. Since $qR \to z$ as $\theta \to 0$, this is very similar to the universality of I vs. q parameterized on ρ shown in Figs. 3 and 4. His result applies for the complete scattering function, not just the envelope, but is limited to small θ and m. The approximate universality on ρ and qR proposed here holds for all θ and m but applies only to the overall structure of the scattering function, i.e., the envelope.

The second approach to describing the Mie scattering envelopes in Fig. 4 is a straightforward Fourier transform. The important concept is that the scattered field is the Fourier transform of only the illuminated portion of the sphere, not necessarily the entire sphere. We again represent the illuminated portion of the sphere as an annular region, and let the inner and outer radii be R_i and R_o. The Fourier transform can be solved analytically to yield

$$I(q)/I(0) = \left[\frac{3}{u^3 - v^3}(\sin u - u\cos u - \sin v + v\cos v)\right]^2 \tag{9a}$$

where

$$u = qR_o \tag{9b}$$

and

$$v = qR_i. \tag{9c}$$

This is just a linear combination of the RDG Eqs. (2a) and (2b) for the two radii. Eq. (9a) is plotted for

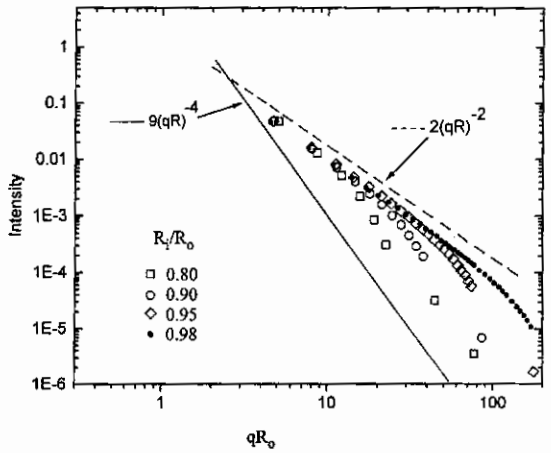

Fig. 7. Envelopes of scattered intensities given by Eq. (9a) for spherical shells of inner and outer radii R_i and R_o, respectively.

$R_i/R_o = 0.8$ in Fig. 6. Readily apparent in Fig. 6 are the three power law regimes, $(qR_o)^0$, $(qR_o)^{-2}$, and $(qR_o)^{-4}$ and a similarity to the complete Mie curves in Fig. 1(b) and Fig. 2(b). The envelopes of Eq. (9a) for $R_i/R_o = 0$, 0.8, 0.9, 0.95, and 0.98 are shown in Fig. 7, and again, the similarity to Mie scattering in Fig. 4 is striking.

4. Comparison to experiment

Here we make a brief comparison to experiment to lend some reality to the computational and theoretical arguments. Most scattering experiments involve ensembles of particles. Any modest polydispersity smears out the interference ripples leaving only the envelopes of the curves [14]. As an example, Fig. 8 displays light scattering data from a water droplet aerosol. Fig. 8(a) shows the data plotted versus θ, Fig. 8(b) vs. q. Plotted versus θ yields no physical interpretation other than enhanced forward scattering; plotted versus q the data are consistent with the three power law regions described herein.

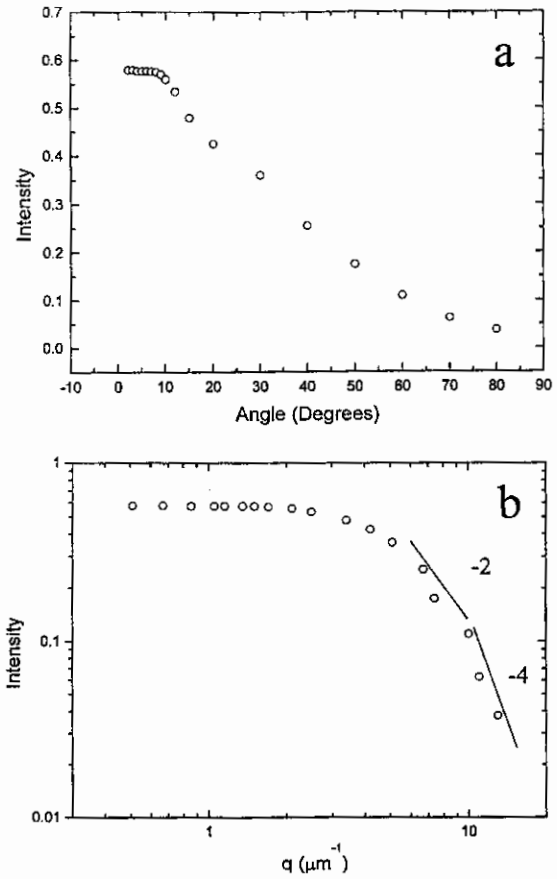

Fig. 8. Light scattering intensity (arbitrary units) from a water droplet aerosol (diameter ≈ 0.5 μm): (a) plotted versus scattering angle; and (b) plotted versus scattering wave vector q. Lines of slope -2 and -4 are drawn.

5. Discussion

The empirical patterns we have found bring some degree of coherency to the complex results of Mie scattering from a sphere. In hindsight, use of q, or better the dimensionless qR, is the obvious choice for the independent variable for examination of the scattered intensity since it is the primary variable in scattering theory. Use of θ follows from experimental convenience, but is not physically motivated. We recommend scattering data always be plotted versus q.

Our model of scattering from a sphere as the Fourier transform of an illuminated annular region with thickness decreasing with increasing ρ is successful in reproducing the major features of the empiricial patterns that we have uncovered. Unfortunately, however, this model is a poor representation of the true internal field. Certainly, at $\rho = 0$ the field is uniform as we assumed. Previous workers have shown that as ρ increases, nonuniformity develops with a tendency for the field to grow at the inner surface. Beyond this, however, our model is much too simple to describe the inner field. Perhaps since we are dealing with only the semiquantitative aspects of the envelopes (not the complete curves) our simplification is enough.

A positive feature of our simple model is that it has allowed us to develop a new conceptualization of scattering which is that the scattering curve is the square of the Fourier transform of the illuminated portion of the scattering object weighted by the amplitude of the illumination. In the language of small angle X-ray [4,5] and neutron scattering [6] we can say that the Mie scattering curve is the structure

factor, but not of the sphere, rather only of the illuminated portion of the sphere.

We conclude with a physical picture of light scattering from a sphere which can be inferred from the results above. At small phase shift parameter ρ, the entire sphere is uniformly illuminated. When q is small (relative to R^{-1}) as well, the waves scattered from all portions of the sphere are in phase hence constructively interfere to give the scattered field with no q dependency. Larger q causes the illuminated interior to scatter waves that in the far field destructively interfere with each other at all finite q (Ewald–Oseen extinction) leaving only a surface boundary (of thickness q^{-1}) to contribute to the scattering. This yields Porod scattering with a $(qR)^{-4}$ dependency. In the other extreme of large ρ the sphere is not uniformly illuminated due to the electromagnetic nature of the wave and the necessary boundary conditions. The low q scattering yields constructive, in-phase addition of all the waves from the illuminated region and no q dependency. Larger q can resolve the illuminated region leading to the $(qR)^{-2}$ dependency. Yet larger q confines the scattering to the surface boundary hence Porods' Law, $(qR)^{-4}$ returns. It is interesting to remark that scattering from the sphere's interior can be eliminated for two reasons, either through Ewald–Oseen extinction of the illuminated interior or through electromagnetic exclusion of the field from the interior. The former leads to surface boundary scattering and Porod's Law, the latter to surface layer scattering and the inverse quadratic dependency.

Acknowledgements

We thank C. Oh for many useful discussions. This paper is dedicated to the memory of Rajiv Pande. This work was supported by NSF Grant CTS 9709764.

References

[1] H.C. van de Hulst, Light Scattering by Small Particles, Dover, New York, 1981.
[2] M. Kerker, The Scattering of Light and other Electromagnetic Radiation, Academic, New York, 1969.
[3] C.F. Bohren, D.R. Huffman, Absorption and Scattering of Light by Small Particles, Wiley, New York, 1983.
[4] A. Guinier, G. Gournet, C.B. Walker, K.L. Yudowitch, Small Angle Scattering of X-Rays, Wiley, New York, 1955.
[5] O. Glatter, O. Kratky (Eds.), Small Angle X-ray Scattering, Academic, New York, 1982.
[6] S.W. Lovesey, Theory of Neutron Scattering from Condensed Matter, Vol. I, Clarendon Press, Oxford, 1994.
[7] C.M. Sorensen, in: K.S. Birdi (Ed.), Handbook of Surface and Colloidal Chemistry, CRC, Boca Raton, FL, 1997.
[8] C. Oh, C.M. Sorensen, J. Nanoparticle Res., in press.
[9] M. Born, E. Wolf, Principles of Optics, Pergamon, Oxford, 1975.
[10] G. Porod, Kolloid Z. 124 (1951) 83.
[11] J.P. Barton, D.R. Alexander, S.A. Schaub, J. Appl. Phys. 65 (1989) 2900.
[12] P.W. Barber, S.C. Hill, Light Scattering by Particles: Computation Methods, World Scientific, Singapore, 1990.
[13] D.Q. Chowdhury, P.W. Barber, S.C. Hill, Appl. Opt. 31 (1992) 3518.
[14] T. Rieker, A. Hanprasapwattana, A. Datye, P. Hubbard, Langmuir 15 (1999) 638.